International Journal of Nanomedicine

Dovepress
open access to scientific and medical research

Open Access Full Text Article

ORIGINAL RESEARCH

A Tf-modified tripterine-loaded coix seed oil microemulsion enhances anti-cervical cancer treatment

This article was published in the following Dove Press journal:
International Journal of Nanomedicine

Yunyan Chen[1–3]
Ding Qu[1,2]
Rongping Fu[1,2]
Mengfei Guo[1,2]
Yue Qin[1,2]
Jian Guo[1,2]
Yan Chen[1,2]

[1]Affiliated Hospital of Integrated Traditional Chinese and Western Medicine, Nanjing University of Chinese Medicine, Nanjing 210028, China; [2]Research Center for Multicomponent of Traditional Chinese Medicine and Microecology, Jiangsu Provincial Academy of Traditional Chinese Medicine, Nanjing 210028, China; [3]Wannan Medical College, Wuhu 241002, China

Purpose: A transferrin-modified microemulsion carrying coix seed oil and tripterine (Tf-CT-MEs) was developed for improved tumor-specific accumulation and penetration to enhance cervical cancer treatment.

Materials and methods: Tripterine-loaded coix seed oil microemulsion (CT-MEs) was prepared through one-step emulsion method. The morphology, size, and zeta potential of CT-MEs and Tf-CT-MEs were examined by transmission electron microscopy and dynamic light scattering. The cellular uptake and mechanisms of HeLa cells were investigated by flow cytometry. Intratumor penetration was investigated using a HeLa three-dimensional (3D) tumor spheroid as the model. The cytotoxicity of the CT-MEs and Tf-CT-MEs against HeLa cells were evaluated by the MTT assay. Additionally, the apoptotic rate of CT-MEs and Tf-CT-MEs inducing apoptosis in HeLa cells was evaluated.

Results: In the physicochemical characterization, coix seed oil and CT-MEs exhibited a small size (32.47±0.15 nm) and nearly neutral surface charge (–0.36±0.11 mV). After modification with transferrin, the particle size of Tf-CT-MEs slightly increased to 40.02±0.21 nm, but the zeta potential decreased remarkably to –13.63±1.31 mV. The IC_{50} of Tf-CT-MEs against HeLa cells was 0.7260 μM, which was 2.58-fold lower than that of CT-MEs. In cellular studies, the intracellular fluorescence intensity of fluorescein isothiocyanate (FITC)-labeled Tf-CT-MEs (FITC/Tf-CT-MEs) was 2.28-fold higher than that of FITC-labeled CT-MEs (FITC/CT-MEs). The fluorescence signal of Tf-CT-MEs was observed at 350 μm below the surface of the 3D tumor spheroid. The apoptotic rate of cells treated with Tf-CT-MEs was 1.73- and 2.77-fold higher than that of cells treated with CT-MEs and tripterine, respectively, which was associated with mitochondrial-targeted delivery of tripterine. Moreover, Tf-CT-MEs was capable of significantly downregulating the cellular level of antiapoptotic proteins and arrested cell proliferation in the G_2/M phase.

Conclusion: Taken together, Tf-CT-MEs holds promising potential to be an efficient drug delivery system for combinational therapy of cervical cancer.

Keywords: tripterine, coix seed oil, microemulsion, deep penetration, anti-cervical cancer

Correspondence: Yan Chen
Research Center for Multicomponent of Traditional Chinese Medicine and Microecology, Jiangsu Provincial Academy of Traditional Chinese Medicine, 100 Shizi Road, Nanjing, Jiangsu 210028, China
Tel +86 25 5236 2155
Fax +86 25 8563 7817
Email ychen202@hotmail.com

Introduction

As reported in a recent survey, cervical cancer is becoming one of the most common malignancies, threatening the survival of women, and it accounts for 50.38% of cancer-associated mortality worldwide.[1] In China, the number of new cervical cancer cases increases by 61,691 every year, accounting for 29.8% of the global cases of cervical cancer.[2] Although the human papillomavirus prophylaxis vaccine has been popularized in recent years, effective reduction in morbidity and mortality remains

submit your manuscript | www.dovepress.com
Dovepress
http://dx.doi.org/10.2147/IJN.S182475

challenging because of limitations such as age, differences in immune response, and the gap between regional economic development.[3,4] The combinational regimen of carboplatin and paclitaxel is considered as the gold standard for the treatment of cervical cancer in clinic and for improving the quality-of-life and prolonging the survival period of patients.[5,6] However, exposure of toxic agents without tumor selectivity to physiological circulation would lead to severe side effects and even premature termination of treatment, which is also a common predicament for most chemotherapeutics.[7]

Tripterine, a triterpenoid component extracted from the root of *Tripterygium wilfordii*, is capable of inhibiting the proliferation of numerous types of cancer cells, such as cervical (HeLa), lung (A549), breast (MCF-7 and MDA-MB-231), and liver (Hep G2) cancer cells.[8–10] The antitumor mechanisms of tripterine involve the upregulation of mitochondrial apoptotic proteins (Bcl-2 and Bax), interference with the expression of nuclear transcription factors (NF-κB), and blocking inflammatory pathways of NF-κB.[11–17] Owing to its potent antitumor and anti-inflammatory activities, tripterine is identified as one of the five most promising natural drugs of the 21st century.[18] Until now, however, no commercial preparation has been used in clinical application due to its poor water solubility and severe systemic toxicity, including sharp weight loss and acute liver damage. To address the above-mentioned issues, nanotechnology is widely used in the field of pharmaceutics for elevating water solubility, improving oral absorption, reducing toxicity against off-target organs, and promoting distribution at the desired sites.[19–29] In our previous studies, we developed a series of coix seed oil-based microemulsions loaded with etoposide, triterpenes, and polysaccharides from different resources that exhibited synergistic anticancer effects on various tumor models. Kanglaite® injection as a commercial formulation of coix seed oil has already been approved as a supplementary drug for chemotherapeutics in various anticancer treatments.[30,31] According to our previous reports, combinational therapy with coix seed oil and chemotherapeutics enhances anticancer efficacy through a collaborative mechanism.[32,33] Inspired by this strategy, we determined the possibility of synergistic antitumor effects after assembling tripterine and coix seed oil into a microemulsion system.

Modifying the surface of nanomolecules with a tumor-targeted ligand can improve drug accumulation at the desired sites, a commonly used and effective method for enhancing efficacy and reducing toxicity of the drug.[34–39] Transferrin receptor (TfR) is a protein that is overexpressed on the surface of many cancer cells at a density that is significantly higher than that of normal cells, making TfR a potential target for specific recognition of tumor cells. As reported previously, transferrin (Tf) acts as an iron ion shuttle in the human body and delivers iron ion payloads into the cells and then locates back to the extracellular environment after transporting iron. Thus, TfR is different from other ligands and hence is the most promising applicable tumor targeting molecule over the past decades.

In this study, we developed a dual-component microemulsion delivery system (transferrin-modified tripterine-loaded coix seed oil microemulsion [Tf-CT-MEs]) comprising tripterine (anticancer drug 1), coix seed oil (anticancer drug 2, in oil phase), RH 40 (surfactant), PEG 400 (cosurfactant), and Tf, which were conjugated with the hydroxyl group of PEG 400 (Scheme 1). Furthermore, the significance of the

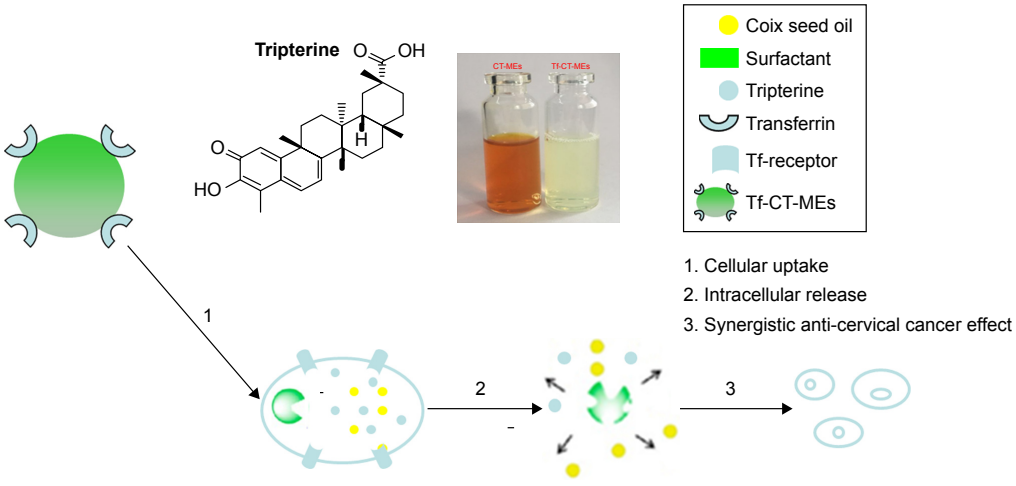

Scheme 1 In this coix seed components-based microemulsion system, coix seed oil was used in the oil phase, and acted as an antitumor ingredient, tripterine as an antitumor component, and Tf as an active targeting ligand was modified on the surface of Tf-CT-MEs.
Abbreviations: Tf, transferrin; Tf-CT-MEs, transferrin-modified tripterine-loaded coix seed oil microemulsion.

combination therapy with tripterine and coix seed oil as a microemulsion system was validated with regard to preparation, characterization, cellular studies, and molecular mechanism. Notably, we employed a HeLa three-dimensional (3D) tumor spheroid model to demonstrate the antitumor activity of Tf-CT-MEs in a microcosmic 3D structure.

Materials and methods

Materials

Tripterine (purity >99.9%) was obtained from Sinopharm Group Co, Ltd (Shanghai, China). Coix seed oil (purity >85%) was extracted by supercritical fluid extraction.[40] Cremophor® RH 40 was provided by BASF Co, Ltd (Ludwigshafen, Germany). PEG 400 was purchased from Sigma-Aldrich Co (St Louis, MO, USA). Tf was purchased from Tufeng Biology Co, Ltd (Shanghai, China). 1-(3-Dimethylaminopropyl)-3-ethylcarbodiimide hydrochloride (EDC) and N-hydroxysuccinimide (NHS) were offered by TCI Development Co, Ltd (Shanghai, China). HeLa cells were purchased from the cell bank of the Chinese Academy of Sciences (Shanghai, China). MTT was sourced from Amresco, Inc (Solon, OH, USA). Amiloride, sucrose, genistein, and ammonium chloride were purchased from Sinopharm Group Co, Ltd. Experimental water was produced by Milli-Q water purification system (Merck Millipore, Billerica, MA, USA). All other chemicals were of analytical grade unless stated otherwise.

Preparation and characterization of microemulsions

Tf-CT-MEs was prepared as follows: 10 mg of tripterine was dissolved in 400 mg of coix seed oil with vigorous stirring at 600 rpm; after mixing for 2 hours, 450 mg of RH 40 and 150 mg of PEG 400 were added in the resultant mixture, followed by further magnetic stirring for 2 hours at 40°C. Next, 10 mL of deionized water was slowly added to obtain a transparent tripterine-loaded coix seed oil microemulsion (CT-MEs) solution. Finally, 50 µL of CT-MEs was dispersed in 3 mL of water, followed by the addition of 0.74 mg of EDC, 0.47 mg of NHS, and 0.55 mg of Tf and reacting for 8 hours. After ultracentrifugation at 20,000×*g* for 20 minutes, pure Tf-CT-MEs was obtained as an orange opalescent solution. The particle size and zeta potential of the microemulsions were measured by dynamic light scattering (DLS) measurement (Nano ZS; Malvern Instruments Ltd, Malvern, UK). The morphology of the microemulsions was observed by transmission electron microscopy (TEM; JEM-200CX; JEOL, Tokyo, Japan) as reported previously.[34]

Drug encapsulation efficiency (EE) and drug loading efficiency (LE) of microemulsions

The EE of tripterine was calculated as follows:

$$EE_{tripterine}(\%) = C \times \frac{V}{W} \times 100\%$$

where C represents the tripterine concentration, V represents the microemulsion volume, and W represents the feeding weight of tripterine.

The LE of tripterine was calculated as follows:

$$LE_{tripterine}(\%) = C \times \frac{V}{W_{\text{freeze-dried microemulsions}}} \times 100\%$$

where C represents the tripterine concentration of freeze-dried microemulsions, V represents the volume of freeze-dried microemulsions reconstituted in water, and W represents the weight of the freeze-dried microemulsions.

The contents of tripterine in CT-MEs and Tf-CT-MEs were determined by HPLC (1260 Infinity; Agilent Technologies, Santa Clara, CA, USA) at 426 nm. The chromatographic conditions were as follows: reversed phase C_{18} column (4.6×150 mm ×5 µm, Diamond); flow rate, 1.0 mL/min; column temperature, 30°C; mobile phase, methanol:water (90:10, v/v).

In vitro drug release

One milliliter of the microemulsion was transferred to a dialysis bag (molecular weight cutoff of 10 kDa), followed by immersion into 120 mL of PBS (pH 7.4) with 0.5% (wt%) Tween 80 at 37°C. Fifty microliters of the medium was eluted at predetermined time intervals and then filtered through a 0.22-µm polycarbonate membrane filter. The concentration of tripterine in the samples and the accumulative release of tripterine from CT-MEs and Tf-CT-MEs were determined by HPLC.

Cell culture

HeLa cells were cultured in a cell incubator with an atmosphere of 5% CO_2 and 95% humidity at 37°C. DMEM culture medium, containing 10% FBS (v/v), 1% streptomycin (100 µg/mL), and penicillin (100 IU/mL), was used for culturing HeLa cells. After reaching 80% confluency, HeLa cells were subcultivated using trypsin at the split ratio of 1:3.

Cellular uptake and intracellular delivery

HeLa cells (1×10^5) were seeded into six-well plates and cultured overnight. After reaching 80% of the overspread, the cells were treated with fluorescein isothiocyanate (FITC)-labeled Tf-CT-MEs (FITC/Tf-CT-MEs) for 4 hours, and FITC and FITC-labeled CT-MEs (FITC/CT-MEs) were considered controls. The concentration of FITC/Tf-CT-MEs and FITC/CT-MEs was calculated as FITC (10 μM). At the end of the incubation, the cells were rinsed with ice-cold PBS thrice, collected using trypsin without EDTA, and then harvested in 0.2 mL of PBS, followed by analysis using flow cytometry (Guava 6HT; Merck Millipore) by counting 5,000 events.

To dissect the mechanism of cellular uptake, several endocytosis pathways were blocked by low temperature and pretreatment with specific uptake inhibitors. Briefly, HeLa cells (1×10^5) were pretreated as follows: 1 mg/mL of Tf, 54 μg/mL of genistein, 154 mg/mL of sucrose, 133 μg/mL of amiloride at 37°C, and FBS-free medium at 4°C for 1 hour. Afterward, the cells were incubated with FITC/Tf-CT-MEs and FITC/CT-MEs in the presence of the above-mentioned inhibitors for further 2 hours. The intracellular intensity was measured by flow cytometry according to a similar method mentioned above.

HeLa cells (1×10^5) were seeded on a polylysine-coated glass sheet (Thermo Fisher Scientific, Waltham, MA, USA) in each well of 24-well plates. After reaching 50% confluence, FITC/CT-MEs and FITC/Tf-CT-MEs were incubated with cells at an FITC concentration of 10 μM for 4 hours. At the end of the incubation, the cells were washed with ice-cold PBS thrice and then stained with 50 nM LysoTracker Red (Abcam, Cambridge, UK) or 100 nM MitoTracker Red CMXRos (Yeasen, China) for 30 minutes at room temperature in the dark. Finally, the cells were fixed by 4% paraformaldehyde for 15 minutes at room temperature, followed by observation by confocal laser scanning microscopy (CLSM).

Cytotoxicity studies

HeLa cells were seeded in 96-well plates with a density of 5×10^3 cells/well and cultured for 24 hours. After reaching 70% of the overspread, the cells were treated with Tf-CT-MEs at predetermined tripterine concentrations; tripterine and CT-MEs were used as controls. After 24-hour incubation, the cells were stained with 10 μL of MTT solution (5 mg/mL) at 37°C for 4 hours. Then, the resultant formazan crystals were dissolved with 100 μL of dimethyl sulfoxide. A microplate reader (Varioskan Flash; Thermo Fisher Scientific) was used to measure the absorbance of formazan crystals at 570 nm. The viability ratio was calculated as follows:

$$\text{Cell viability (\%)} = \frac{\text{OD of test}}{\text{OD of control}}.$$

Preparation of 3D tumor spheroids[41]

HeLa cells (1×10^3) were seeded on the surface of an agarose-based culture medium in 96-well plates at 37°C under an atmosphere of 5% CO_2. After 10-day incubation, HeLa 3D tumor spheroids with intact spherical structure and proper size were selected for the following studies. The images of tumor spheroids were acquired by CLSM. Prior to the experiment, HeLa 3D tumor spheroids with similar size were selected and transferred to confocal dishes. Thereafter, the HeLa 3D tumor spheroids were treated with FITC/CT-MEs and FITC/Tf-CT-MEs at an FITC concentration of 10 μM for 12 hours at 37°C, followed by fixing with 4% (v%) paraformaldehyde. The samples were observed by CLSM with Z-stack tool (10 μm interval/scan) after washing adequately with PBS.

Toxicity of microemulsions against 3D tumor spheroids

The cytotoxicity of the microemulsions against HeLa 3D tumor spheroids was investigated using the cell counting kit-8 (CCK-8) staining method.[41] Briefly, CT-MEs and Tf-CT-MEs at predetermined concentrations were incubated with HeLa 3D tumor spheroids for 24 hours. Then, the cells were incubated with CCK-8 for further 4 hours. The absorbance of each group was recorded at 450 nm, and cell viability (%) was calculated. In addition, the size of HeLa 3D tumor spheroids was measured once every 2 days during treatment. The area of tumor spheroids was calculated by using the following formula:

$$a\times b\times\frac{\pi}{4},$$

where a and b are the length and width of HeLa 3D tumor spheroids, respectively. After administration of CT-MEs and Tf-CT-MEs for 14 days, HeLa 3D tumor spheroids were collected and fixed with 4% (v%) paraformaldehyde. For H&E staining, HeLa 3D tumor spheroids were visualized using a microscope (VHY-700; Olympus Corporation, Tokyo, Japan). The morphology of HeLa 3D tumor spheroids was observed by FE-SEM (field emission scanning electron

microscope; Zeiss Ultra 55; Carl Zeiss Meditec AG, Jena, Germany).

Cell apoptosis assay

Based on a previous method,[33] 50 µL of HeLa cell suspension containing 5,000 cells was collected and then incubated with 50 µL of Annexin V-PE staining kit (Guava; Merck Millipore) for 15 minutes. The cell suspensions were immediately analyzed by flow cytometry.

Western blot assay

HeLa cells (2×10^3) were treated with Tf-CT-MEs at the tripterine concentration of 2 µg/mL at 37°C, and tripterine, CT-MEs, and FBS-free medium were used as controls. After incubation for 24 hours, the cells were rinsed three times with ice-cold PBS and incubated with lysis buffer (CWBIO, China) for 2 minutes, followed by homogenization of the resultant mixture and ice-cold centrifugation at 13,000×*g* for 10 minutes. The amount of cell protein was quantified using a bicinchoninic acid assay detection kit (Thermo Fisher Scientific).[42] Twenty micrograms of cell proteins were subjected to electrophoresis in SDS-PAGE gels. A polyvinylidene difluoride (PVDF) membrane was then immersed in the transfer buffer for 1.5 hours at 4°C. The PVDF membranes were blocked with 5% nonfat dry milk in TBST buffer for 1 hour at room temperature and then probed with a 1:1,000 dilution of polyclonal antibody against Cell Signaling Technology (caspase-3, Bax, Bcl-2, and GAPDH) for 12 hours at 4°C. After washing three times in TBST, the membranes were incubated in a 1:10,000 dilution of secondary antibody (DyLight™ 800) for 1 hour at room temperature. GAPDH was selected as the loading control. The Odyssey Infrared Imaging system was used for visualization. The experiments were repeated three times.

Cell cycle analysis

The cell cycle was investigated using the propidium iodide (PI) DNA staining method as reported earlier.[43] Briefly, 2×10^5 HeLa cells were seeded in six-well plates and cultured until 70% confluency. Two types of microemulsions with predetermined concentrations (2 µg/mL) were incubated with the cells for 48 hours, harvested as a cell suspension, fixed using ice-cold 75% ethanol, centrifuged at 1,200 rpm for 10 minutes, and washed with ice-cold PBS. Next, the cells were resuspended in 0.5 mL of PI/RNase staining solution for 15 minutes at room temperature in the dark. The samples were immediately analyzed by flow cytometry.

Statistical analysis

Statistical significance was tested by the two-tailed Student's *t*-test. It was defined as $*P<0.05$, and extreme statistical significance was defined as $**P<0.01$. Data are shown as mean ± SD.

Results and discussion

Preparation and characterization

CT-MEs was prepared through the one-step emulsion method as reported previously, and Tf-CT-MEs was assembled via covalent linkage of PEG 400 and Tf.[44] As shown in Figure 1A, the particle size of Tf-CT-MEs was ~40 nm, which was slightly larger than that of CT-MEs. The zeta potential of Tf-CT-MEs was moderately negative (~−14 mV), which was distinct from that of CT-MEs (only −0.357 mV). This difference was attributed to the modification of Tf on the surface of the microemulsion.[37] As depicted in Figure 1B, the EEs of Tf-CT-MEs and CT-MEs were 94.50% and 98.55%, respectively. Likewise, there was no obvious difference in tripterine LE between the two types of microemulsions, and the total LE of Tf-CT-MEs and CT-MEs were 40.973% and 40.773%, respectively. The LE of tripterine in CT-MEs and Tf-CT-MEs is shown in Figure S1. Figure 1C displays the morphology of the microemulsions. CT-MEs had a spherical structure with a particle size of 30 nm and narrow size dispersion. In contrast, the edge of Tf-CT-MEs was irregular, probably associated with the modification of Tf. The results of TEM were in line with DLS results as described above. As shown in Figure 1D, 40% of the tripterine was released from CT-MEs during the initial 4 hours, which was slightly slower (but not statistically different) than that of Tf-CT-MEs in PBS, pH 7.4. With the increase in time, at 24 hours, the accumulative release was 62.21% and 50.21% from Tf-CT-MEs and CT-MEs, respectively, suggesting that Tf modification did not influence the release profile in the physiological environment. Collectively, Tf-CT-MEs represent nanosized monodispersed particles and are strongly compatible for water-insoluble drugs and exhibit good potential stability in vivo.

Cellular uptake assay of CT-MEs and Tf-CT-MEs

In the cellular uptake study, we qualitatively and quantitatively evaluated the uptake to demonstrate the advantage of Tf modification. As shown in Figure 2A and B, the intracellular fluorescence of both types of microemulsions was more intensive compared with that of the free FITC group, suggesting the inherent advantage of nanosized particles on

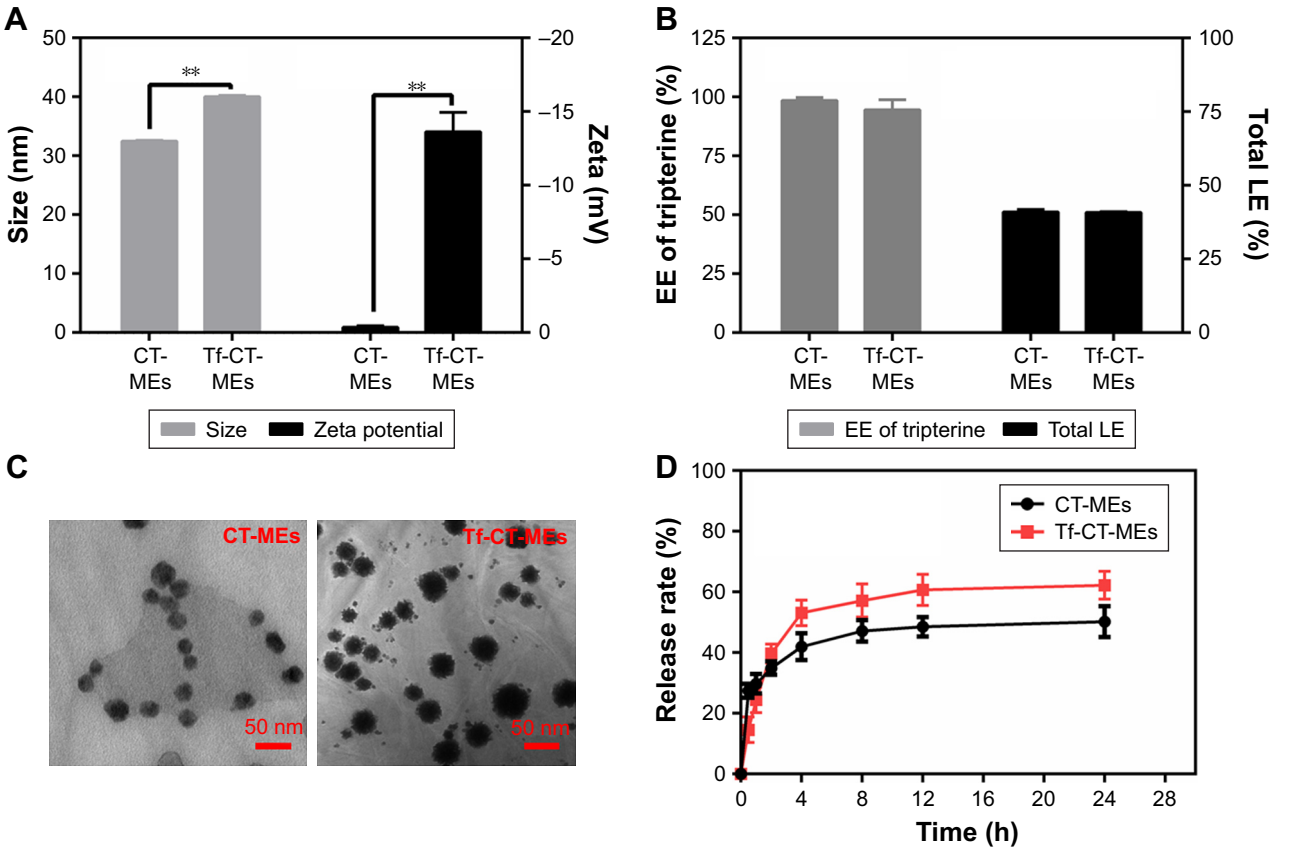

Figure 1 Characterization of microemulsions.
Notes: (**A**) Particle size and zeta potential of CT-MEs and Tf-CT-MEs. $^{**}P<0.01$ (n=3). (**B**) Drug EE and drug LE of CT-MEs and Tf-CT-MEs (n=3). (**C**) TEM images of CT-MEs and Tf-CT-MEs. Scale bar: 50 nm. (**D**) Release profile of CT-MEs and Tf-CT-MEs (n=3).
Abbreviations: CT-MEs, tripterine-loaded coix seed oil microemulsion; EE, encapsulation efficiency; LE, loading efficiency; TEM, transmission electron microscopy; Tf-CT-MEs, transferrin-modified tripterine-loaded coix seed oil microemulsion.

internalization. Notably, the fluorescence intensity of Tf-CT-MEs was 2.28-fold higher than that of CT-MEs, indicating Tf-mediated enhancement of endocytosis.

The intracellular transport of the microemulsion was observed by CLSM. To determine the potential distribution of microemulsions after crossing the cell membrane, lysosomes were stained with a red fluorescent dye (LysoTracker Red), and microemulsions were labeled with a green fluorescent dye (FITC).[44] As shown in Figure 2C, cells treated with FITC/Tf-CT-MEs were observed as obvious yellow fluorescence, indicating that the microemulsions were probably entrapped by endo/lysosomes. According to previous reports, tripterine suppresses the proliferation of tumor cells via the mitochondrial apoptosis pathway.[11–17] However, whether mitochondrial-targeted delivery of tripterine could amplify the apoptotic effect is not yet known. As shown in Figure 2D, the mitochondria were stained with red fluorescence (MitoTracker Red) and the formulation was labeled with green fluorescence (FITC). Interestingly, the cells treated with FITC/Tf-CT-MEs displayed the obvious overlap of red and green fluorescence, which represented co-localization of the mitochondria and microemulsions. However, FITC/CT-MEs was rarely distributed at the mitochondria, which was probably because of the neutral charge. The uptake dynamics and mechanisms of HeLa cells were investigated by flow cytometry. As shown in Figure 2E, the cells required 4 hours to reach the cellular uptake platform period. Amiloride, sucrose, and genistein were used as specific inhibitors for macropinocytosis, clathrin-mediated endocytosis, and caveolae-mediated endocytosis, respectively (Figure 2F). The experimental conditions of incubation at 4°C significantly inhibited the internalization of CT-MEs and Tf-CT-MEs, suggesting that CT-MEs and Tf-CT-MEs entered HeLa cells in an energy-dependent pathway. Incubation of CT-MEs and Tf-CT-MEs with HeLa cells significantly reduced cell uptake in the presence of sucrose, indicating that clathrin is involved in the internalization. However, cellular uptake of Tf-CT-MEs decreased significantly in the presence of Tf, indicating that Tf-CT-MEs was internalized by HeLa cells via the TfR-mediated pathway.

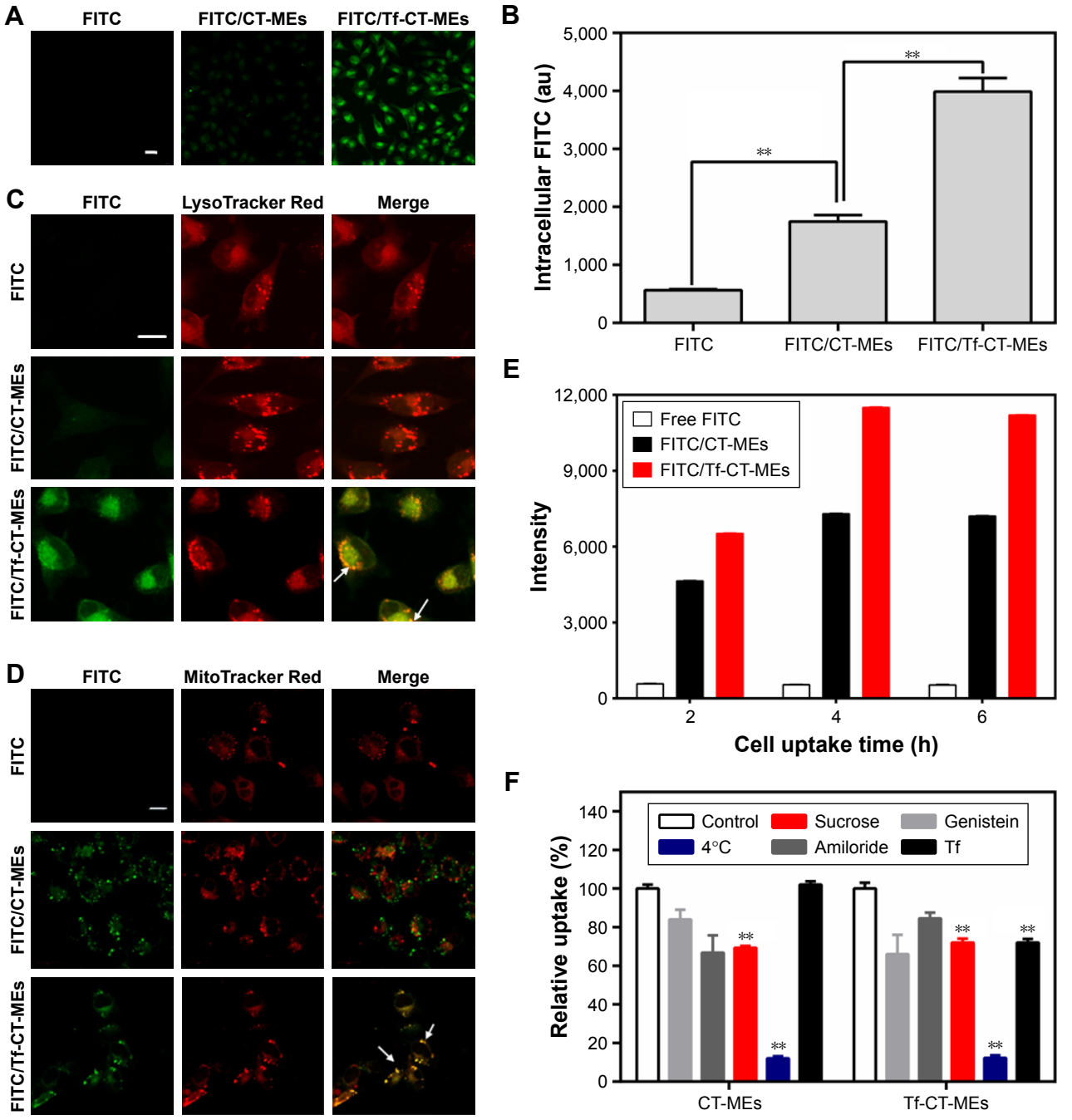

Figure 2 (**A**) Fluorescence images of HeLa cells treated with various formulations. Scale bar: 50 μm. (**B**) Quantitation of intracellular green fluorescence intensity measured using flow cytometry (n=3). $^{**}P<0.01$. Intracellular delivery of CT-MEs and Tf-CT-MEs within HeLa cells observed using CLSM. The arrows represent Tf-CT-MEs entrapped in the (**C**) endo/lysosomes and (**D**) mitochondria. Scale bar: 25 μm. (**E**) Uptake kinetics study. Quantitation of intracellular green fluorescence intensity measured using flow cytometry (n=3). (**F**) Relative uptake efficiency of CT-MEs and Tf-CT-MEs after pretreating HeLa cells with different endocytosis inhibitors (n=3). $^{**}P<0.01$.

Abbreviations: CLSM, confocal laser scanning microscopy; CT-MEs, tripterine-loaded coix seed oil microemulsion; FITC, fluorescein isothiocyanate; FITC/CT-MEs, FITC-loaded coix seed oil microemulsion; FITC/Tf-CT-MEs, FITC-loaded transferrin-modified coix seed oil microemulsion; Tf, transferrin; Tf-CT-MEs, transferrin-modified tripterine-loaded coix seed oil microemulsion.

Tumor penetration and treatment

CT-MEs and Tf-CT-MEs formulated with small size were supposed to demonstrate enhanced performance of tumor penetration.[45] To verify whether the tumor penetration capacity of CT-MEs and Tf-CT-MEs was improved, we observed the distribution of CT-MEs and Tf-CT-MEs in HeLa 3D tumor spheroids. As shown in Figure 3A, we observed that both CT-MEs and Tf-CT-MEs exhibited enhanced performance of tumor penetration, with distribution at a depth of 350 μm in HeLa 3D tumor spheroids

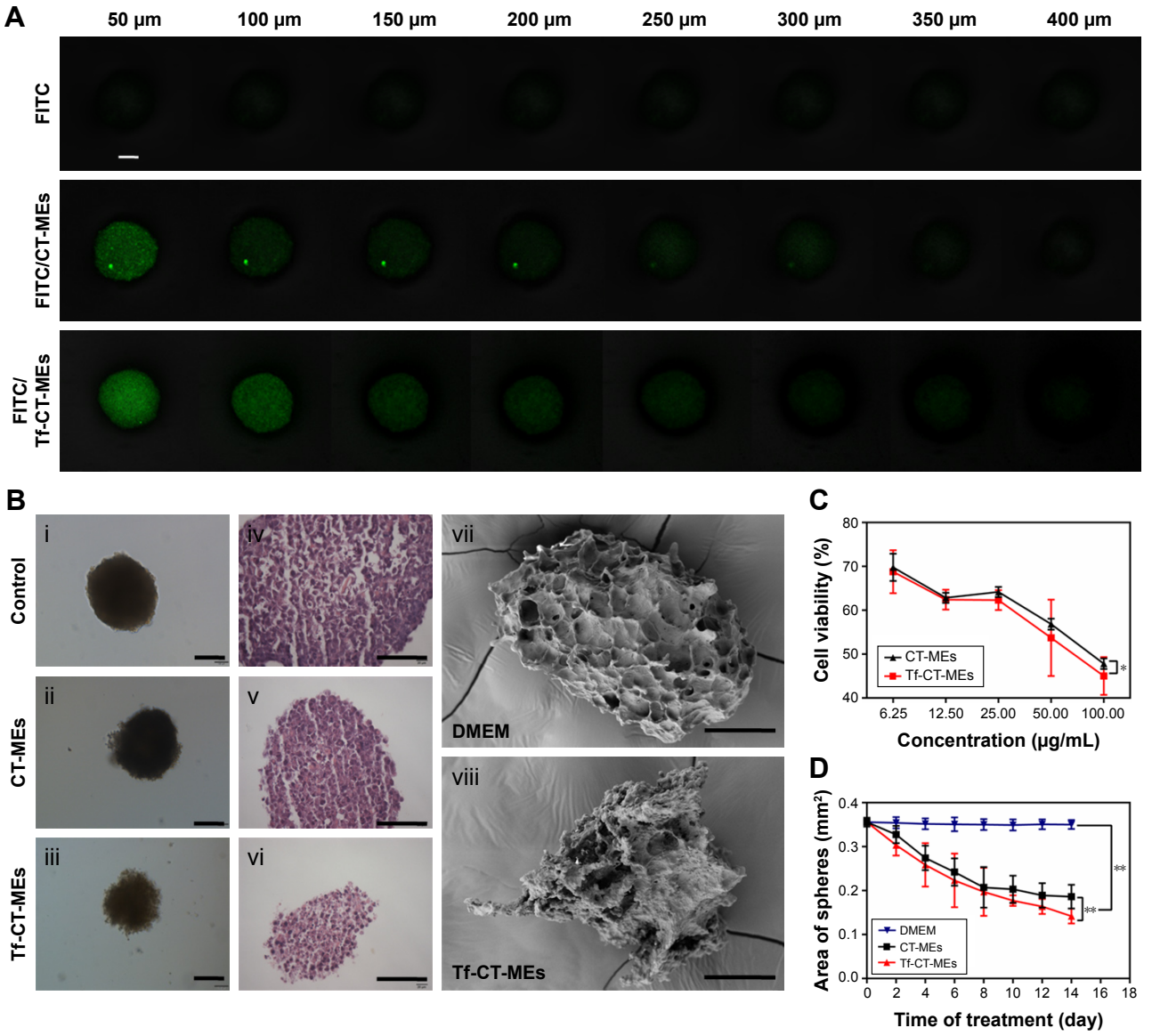

Figure 3 (**A**) Evaluation on the penetration of CT-MEs and Tf-CT-MEs using HeLa 3D tumor spheres model. The green color represents the penetrated CT-MEs and Tf-CT-MEs. Scale bar: 100 μm. (**B**) Characterization of the HeLa 3D tumor spheres treated with DMEM, CT-MEs, and Tf-CT-MEs (200 μg/mL) for 24 hours by light microscope (i–iii). Besides, H&E staining (iv–vi) and FE-SEM (vii, viii) of HeLa 3D tumor spheres were also performed. Scale bar: 100 μm. (**C**) Viability of the HeLa 3D tumor spheres treated with CT-MEs and Tf-CT-MEs after 24 hours using CCK-8 (n=6). *$P<0.05$. (**D**) Area of the HeLa 3D tumor spheres treated with CT-MEs and Tf-CT-MEs for 14 days (n=6). **$P<0.01$.

Abbreviations: CCK-8, cell counting kit-8; CT-MEs, tripterine-loaded coix seed oil microemulsion; FE-SEM, field emission scanning electron microscope; Tf-CT-MEs, transferrin-modified tripterine-loaded coix seed oil microemulsion.

(diameter of ~500 μm). Tf-CT-MEs exhibited advantageous penetration, which may be due to its particle size, and Tf modification led to the enhancement of cellular uptake. Thus, Tf-CT-MEs verified that particle size is an advantage of microemulsions, as previously reported.[46]

As shown in Figure 3B(i), HeLa 3D tumor spheroids with a diameter of ~500 μm were compact and spherical after culture for 10 days. Microscopic images of HeLa 3D tumor spheroids after treatment with CT-MEs and Tf-CT-MEs (200 μg/mL) for 24 hours are shown in Figure 3B(ii) and (iii). H&E staining was performed 14 days after administration of Tf-CT-MEs and CT-MEs as shown in Figure 3B(iv)–(vi). The results indicated that nanosized microemulsions can penetrate into HeLa 3D tumor spheroids to release tripterine to destroy the structure of HeLa 3D tumor spheroids.[47] Figure 3B(viii) shows the FE-SEM image of the structural damage to HeLa 3D tumor spheroids after administration of Tf-CT-MEs and HeLa 3D tumor spheroids treated with DMEM is shown in Figure 3B(vii).

We further investigated the cytotoxicity of CT-MEs and Tf-CT-MEs against HeLa 3D tumor spheroids. We observed dramatically lower cytotoxicity with IC_{50} values of 100.7 and

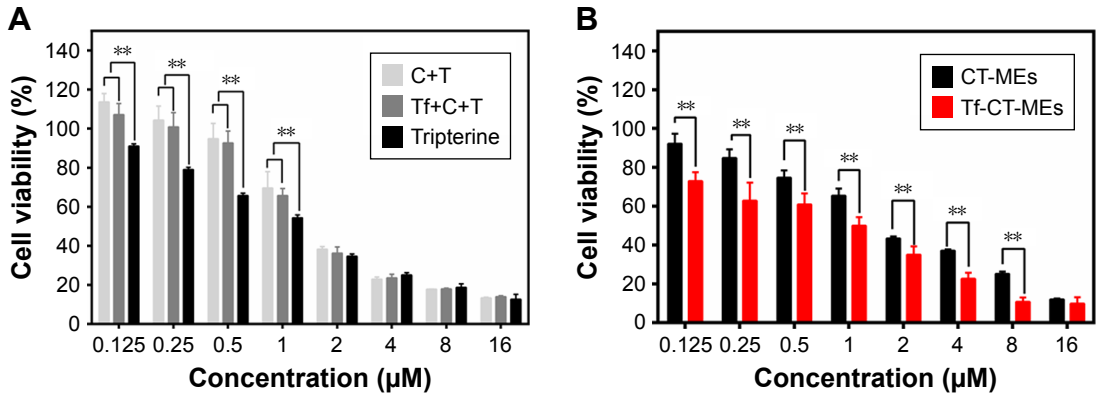

Figure 4 Antiproliferative effects of CT-MEs and Tf-CT-MEs formulations against HeLa cells for 24 hours by MTT method (n=6). $^{**}P<0.01$.
Note: Antiproliferative effects of (**A**) excipients and (**B**) CT-MEs and Tf-CT-MEs formulations.
Abbreviations: CT-MEs, tripterine-loaded coix seed oil microemulsion; Tf-CT-MEs, transferrin-modified tripterine-loaded coix seed oil microemulsion; T, Tripterine; C, coix seed oil.

79.60 μg/mL for CT-MEs and Tf-CT-MEs, respectively, against HeLa 3D tumor spheroids (Figure 3C). The low cytotoxicity was primarily because of the lower uptake of tripterine by HeLa 3D tumor spheroids.

We also validated the antitumor effect of CT-MEs and Tf-CT-MEs by determining the area reduction of HeLa 3D tumor spheroids after the 14-day treatment. As shown in Figure 3D, a reduction in the area of HeLa 3D tumor spheroids was observed after treatment with CT-MEs and Tf-CT-MEs. Notably, the reduction area by Tf-CT-MEs was 1.31-fold higher than that by CT-MEs, indicating that Tf-CT-MEs exhibited better anti-cervical cancer efficacy in HeLa 3D tumor spheroids.

Antiproliferative effects in vitro

The cytotoxicity of CT-MEs and Tf-CT-MEs against HeLa cells was evaluated by the MTT assay after 24 hours (Figure 4). We observed concentration-dependent antiproliferative activity of CT-MEs, Tf-CT-MEs, and the mixture when the concentration of tripterine was increased from 0.125 to 16 μM. IC_{50} values of CT-MEs and Tf-CT-MEs against HeLa cells were ~1.876±0.2020 and 0.7260±0.1520 μM, respectively. The IC_{50} value of Tf-CT-MEs was 2.58-fold lower than that of CT-MEs, illustrating the enhancement of cytotoxicity after Tf modification.

Induction of apoptosis

Based on the results of the MTT assay and CCK-8 test (Figures 3C and 4B), both CT-MEs and Tf-CT-MEs should be able to induce HeLa cell apoptosis. To confirm this design strategy, we used an Annexin V-PE cell apoptosis detection kit to detect apoptosis induction by tripterine, CT-MEs, and Tf-CT-MEs (Figure 5A).[34] There was a significant difference between CT-MEs and Tf-CT-MEs in the total apoptosis rate.

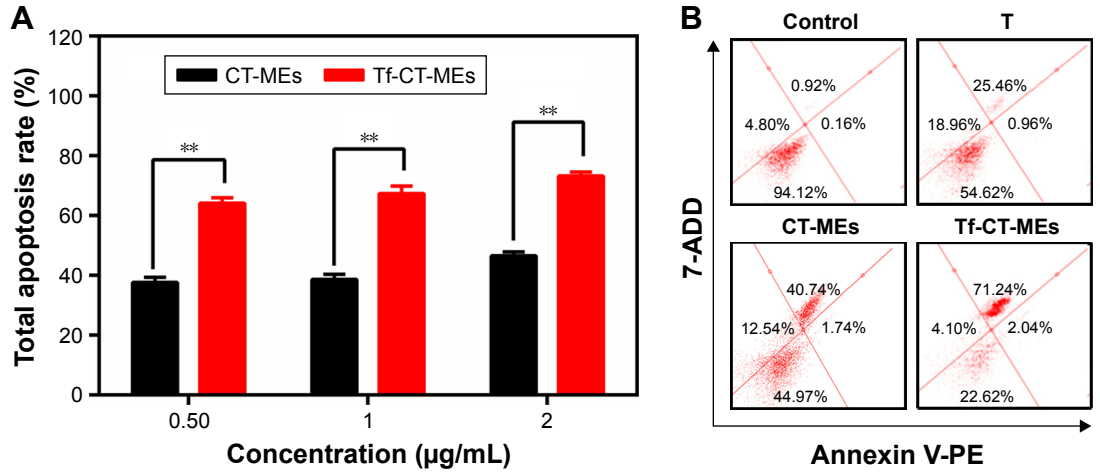

Figure 5 Cytotoxicity of different treatments against HeLa cells for 4 hours.
Notes: (**A**) The quantification of cell apoptosis rate after various treatments of formulations. $^{**}P<0.01$. (**B**) In each quadrant of apoptosis, the upper right and lower right zones represent late apoptosis and early apoptosis, respectively (n=3).
Abbreviations: CT-MEs, tripterine-loaded coix seed oil microemulsion; Tf-CT-MEs, transferrin-modified tripterine-loaded coix seed oil microemulsion; T, Tripterine; 7-ADD, 7-amino-actinomycin D; PE, phycoerythin.

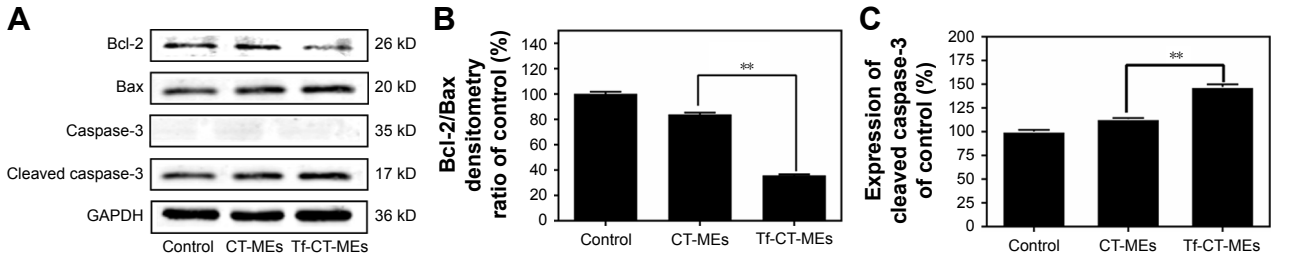

Figure 6 (**A**) Expression of Bcl-2, Bax, caspase-3, and cleaved caspase-3 proteins was detected in HeLa cells by Western blot analysis. (**B**) Ratio of Bcl-2/Bax of each group normalized to control (n=3). (**C**) Ratio of cleaved caspase-3 normalized to control (n=3). $^{**}P<0.01$ vs control.
Abbreviations: CT-MEs, tripterine-loaded coix seed oil microemulsion; Tf-CT-MEs, transferrin-modified tripterine-loaded coix seed oil microemulsion.

As shown in Figure 5B, the results indicated that at the concentration of 2 μg/mL, tripterine induced significant apoptosis compared with that by the negative control after treatment for 4 hours. Interestingly, we found that Tf-CT-MEs exhibited more significant ability to enhance apoptosis than that by CT-MEs, which may be due to the function of the Tf modification. Compared to CT-MEs (42.48%±1.34%) and tripterine (26.42%), Tf-CT-MEs (73.28%) exhibited 1.73- and 2.77-fold higher apoptosis rate, respectively. When HeLa cells were administered with a mixture of coix seed oil and tripterine, the synergistic effect suddenly declined (Figure S2).

Western blot

The action mechanisms of CT-MEs- and Tf-CT-MEs-induced cell apoptosis on HeLa cells were elaborated in this study. Typically, there are two main pathways of cell apoptosis, the extrinsic and intrinsic apoptotic pathways.[47] HeLa cells were treated with CT-MEs, Tf-CT-MEs, and DMEM (as the control) for 24 hours; the total cellular protein was then extracted. The Western blot results are shown in Figure 6A. In contrast with the control group, the expression of Bcl-2/Bax was downregulated in HeLa cells (Figure 6B), but the expression of cleaved caspase-3 was significantly upregulated (Figure 6C) which indicated that CT-MEs and Tf-CT-MEs induced apoptosis in HeLa cells via the intrinsic apoptotic pathway.[48,49]

Cell cycle analysis

Antitumor drugs primarily block tumor cells in three phases of cell cycle, viz G_0/G_1, S, and G_2/M.[50–54] In our study, the effects of CT-MEs and Tf-CT-MEs on cell cycle progression were determined by flow cytometry. Here, we experimentally determined the IC_{50} value of various formulations. Compared to the control group, we found a significant increase in the percentage of the G_2 phase after treatment with CT-MEs and Tf-CT-MEs. As shown in Figure 7A, compared with the control group (19.41%), the percentage of G_2 increased significantly to 39.73% and 35.47% when HeLa cells were treated with CT-MEs and Tf-CT-MEs, respectively, for 24 hours. According to the statistical results in Figure 7B, the inhibition of cell growth caused an increase

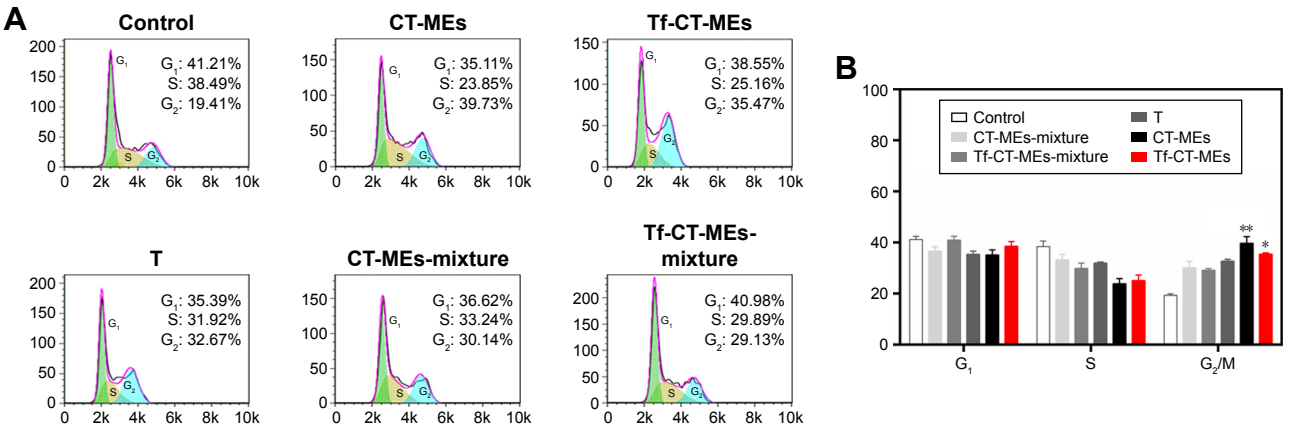

Figure 7 (**A**) Flow cytometry analysis of cell cycle phase distribution in HeLa cells. (**B**) Bar diagram showing the cell distribution in the G_1, S, and G_2/M phases for HeLa cells treated with different formulations (n=3). $^{*}P<0.05$; $^{**}P<0.01$.
Abbreviations: CT-MEs, tripterine-loaded coix seed oil microemulsion; Tf-CT-MEs, transferrin-modified tripterine-loaded coix seed oil microemulsion; T, Tripterine.

in HeLa cells in the G_2 phase, which subsequently induced cell apoptosis.

Conclusion

In this study, we developed a dual-component microemulsion delivery system by combining coix seed oil and tripterine for cervical cancer treatment. Tf-CT-MEs with small particle size (40.02±0.21 nm) and neutral potential (−13.63±1.31 mV) exhibited high cytotoxicity and improved apoptosis induction in HeLa cells. In particular, Tf-CT-MEs exhibited more enhanced cellular uptake after Tf modification. The small size of Tf-CT-MEs enhanced tumor penetration in HeLa 3D tumor spheroids. H&E staining and FE-SEM illustrated that Tf-CT-MEs exhibited excellent antitumor activity in vitro. Western blot obviously demonstrated that the apoptotic degree of Tf-CT-MEs was higher than that of CT-MEs. We believe that Tf-CT-MEs is promising and an efficient drug delivery system for cervical cancer treatment, and its simple preparation process enables its availability as a commercial product.

Acknowledgment

This work was supported financially by the National Natural Science Foundation of China (81673606, 81873017), Science and Key Medical Talent Project of Jiangsu Province (ZDRCA2016036), the "333 High-Level Talents Training Project" of Jiangsu Province (BRA2016506), and the Key Medical Youth Talent Project of Jiangsu Province (QNRC2016631).

Disclosure

The authors report no conflicts of interest in this work.

References

1. World Health Organization (2014) GLOBOCAN2012: Estimated Cancer Incidence, Mortality and Prevalence Worldwide in 2012. Available from: http://globocan.iarc.fr/Default.aspx. Accessed December 1, 2014.
2. Torre LA, Bray F, Siegel RL, Ferlay J, Lortet-Tieulent J, Jemal A. Global cancer statistics, 2012. *CA Cancer J Clin*. 2015;65(2):87–108.
3. Joura EA, Giuliano AR, Iversen OE, et al. A 9-valent HPV vaccine against infection and intraepithelial neoplasia in women. *N Engl J Med*. 2015;372(8):711–723.
4. Kirby T. FDA approves new upgraded Gardasil 9. *Lancet Oncol*. 2015;16(2):56.
5. Kitagawa R, Katsumata N, Ando M, et al. A multi-institutional phase II trial of paclitaxel and carboplatin in the treatment of advanced or recurrent cervical cancer. *Gynecol Oncol*. 2012;125(2):307–311.
6. Singh S, Dash AK. Paclitaxel in cancer treatment: perspectives and prospects of its delivery challenges. *Crit Rev Ther Drug Carrier Syst*. 2009;26(4):333–372.
7. Medina C, Santos-Martinez MJ, Radomski A, Corrigan OI, Radomski MW. Nanoparticles: pharmacological and toxicological significance. *Br J Pharmacol*. 2010;150(5):552–558.
8. Sha M, Ye J, Zhang LX, Luan ZY, Chen YB, Huang JX. Celastrol induces apoptosis of gastric cancer cells by miR-21 inhibiting PI3K/Akt-NF-κB signaling pathway. *Pharmacology*. 2014;93(1–2):39–46.
9. Mou H, Zheng Y, Zhao P, Bao H, Fang W, Xu N. Celastrol induces apoptosis in non-small-cell lung cancer A549 cells through activation of mitochondria- and Fas/FasL-mediated pathways. *Toxicol In Vitro*. 2011;25(5):1027–1032.
10. Wang WB, Feng LX, Yue QX, et al. Paraptosis accompanied by autophagy and apoptosis was induced by celastrol, a natural compound with influence on proteasome, ER stress and Hsp90. *J Cell Physiol*. 2012;227(5):2196–2206.
11. Dai Y, Desano J, Tang W, et al. Natural proteasome inhibitor celastrol suppresses androgen-independent prostate cancer progression by modulating apoptotic proteins and NF-kappaB. *PLoS One*. 2010;5(12):e14153.
12. Kim Y, Kang H, Jang SW, et al. Celastrol inhibits breast cancer cell invasion via suppression of NF-κB-mediated matrix metalloproteinase-9 expression. *Cell Physiol Biochem*. 2011;28(2):175–184.
13. Sha M, Ye J, Zhang LX, Luan ZY, Chen YB. Celastrol induces apoptosis of gastric cancer cells by miR-146a inhibition of NF-κB activity. *Cancer Cell Int*. 2013;13(1):50.
14. Chang W, He W, Li PP, et al. Protective effects of Celastrol on diethylnitrosamine-induced hepatocellular carcinoma in rats and its mechanisms. *Eur J Pharmacol*. 2016;784:173–180.
15. Choi JY, Ramasamy T, Kim SY, et al. PEGylated lipid bilayer-supported mesoporous silica nanoparticle composite for synergistic co-delivery of axitinib and celastrol in multi-targeted cancer therapy. *Acta Biomater*. 2016;39:94–105.
16. Wang Z, Zhai Z, Du X. Celastrol inhibits migration and invasion through blocking the NF-κB pathway in ovarian cancer cells. *Exp Ther Med*. 2017;14(1):819–824.
17. Wu J, Ding M, Mao N, et al. Celastrol inhibits chondrosarcoma proliferation, migration and invasion through suppression CIP2A/c-MYC signaling pathway. *J Pharmacol Sci*. 2017;134(1):22–28.
18. Corson TW, Crews CM. Molecular understanding and modern application of traditional medicines: triumphs and trials. *Cell*. 2007;130(5):769–774.
19. Morton SW, Lee MJ, Deng ZJ, et al. A nanoparticle-based combination chemotherapy delivery system for enhanced tumor killing by dynamic rewiring of signaling pathways. *Sci Signal*. 2014;7(325):44.
20. Wang H, Zhao Y, Wu Y, et al. Enhanced anti-tumor efficacy by co-delivery of doxorubicin and paclitaxel with amphiphilic methoxy PEG-PLGA copolymer nanoparticles. *Biomaterials*. 2011;32(32):8281–8290.
21. Xiong XB, Lavasanifar A. Traceable multifunctional micellar nanocarriers for cancer-targeted co-delivery of MDR-1 siRNA and doxorubicin. *ACS Nano*. 2011;5(6):5202–5213.
22. Guo H, Li F, Xu W, et al. Mucoadhesive cationic polypeptide nanogel with enhanced penetration for efficient intravesical chemotherapy of bladder cancer. *Adv Sci*. 2018;5(6):1800004.
23. Zhang Y, Cai L, Li D, et al. Tumor microenvironment-responsive hyaluronate-calcium carbonate hybrid nanoparticle enables effective chemotherapy for primary and advanced osteosarcomas. *Nano Res*. 2018;11(9):4806–4822.
24. Jiang Z, Chen J, Cui L, et al. Advances in Stimuli-Responsive Polypeptide Nanogels. *Small Methods*. 2018;2(3):1700307.
25. Xiao H, Yan L, Dempsey EM, et al. Recent progress in polymer-based platinum drug delivery systems. *Prog Polym Sci*. 2018;87:70–106.
26. Zhang Y, Wang F, Li M, et al. Self-Stabilized Hyaluronate Nanogel for Intracellular Codelivery of Doxorubicin and Cisplatin to Osteosarcoma. *Adv Sci*. 2018;5(5):1700821.
27. Li S, Zhang T, Xu W, et al. Sarcoma-Targeting Peptide-Decorated Polypeptide Nanogel Intracellularly Delivers Shikonin for Upregulated Osteosarcoma Necroptosis and Diminished Pulmonary Metastasis. *Theranostics*. 2018;8(5):1361–1375.
28. Zhao K, Li D, Xu W, et al. Targeted hydroxyethyl starch prodrug for inhibiting the growth and metastasis of prostate cancer. *Biomaterials*. 2017;116:82–94.
29. Chen J, Ding J, Wang Y, et al. Sequentially Responsive Shell-Stacked Nanoparticles for Deep Penetration into Solid Tumors. *Adv Mater*. 2017;29(32):1701170.

30. Wu Y, Zhang J, Hong Y, Wang X. Effects of Kanglaite Injection on Serum miRNA-21 in Patients with Advanced Lung Cancer. *Med Sci Monit*. 2018;24:2901–2906.
31. Wang B, Chen HW, Xuewen L, et al. Clinical effect of Kanglaite injection on chemotherapy of gynecological malignant tumor. *Clin Med*. 2017;37(1):38–39.
32. Qu D, Ma Y, Sun W, et al. Microemulsion-based synergistic dual-drug codelivery system for enhanced apoptosis of tumor cells. *Int J Nanomedicine*. 2015;10(1):1173–1187.
33. Qu D, Wang L, Liu M, et al. Oral Nanomedicine Based on Multicomponent Microemulsions for Drug-Resistant Breast Cancer Treatment. *Biomacromolecules*. 2017;18(4):1268–1280.
34. Wong SM, Kellaway IW, Murdan S. Enhancement of the dissolution rate and oral absorption of a poorly water soluble drug by formation of surfactant-containing microparticles. *Int J Pharm*. 2006;317(1):61–68.
35. Chen J, Ding J, Xu W, et al. Receptor and microenvironment dual-recognizable nanogel for targeted chemotherapy of highly metastatic malignancy. *Nano Lett*. 2017;17(7):4526–4533.
36. Patravale VB, Date AA, Kulkarni RM, Kulkami R. Nanosuspensions: a promising drug delivery strategy. *J Pharm Pharmacol*. 2004;56(7):827–840.
37. Mulik RS, Mönkkönen J, Juvonen RO, Mahadik KR, Paradkar AR. Transferrin mediated solid lipid nanoparticles containing curcumin: enhanced in vitro anticancer activity by induction of apoptosis. *Int J Pharm*. 2010;398(1–2):190–203.
38. Suzuki R, Takizawa T, Kuwata Y, et al. Effective anti-tumor activity of oxaliplatin encapsulated in transferrin-PEG-liposome. *Int J Pharm*. 2008;346(1–2):143–150.
39. Matsubara T, Otani R, Yamashita M, Maeno H, Nodono H, Sato T. Selective Intracellular Delivery of Ganglioside GM3-Binding Peptide through Caveolae/Raft-Mediated Endocytosis. *Biomacromolecules*. 2017;18(2):355–362.
40. Qu D, He J, Liu C, Zhou J, Chen Y. Triterpene-loaded microemulsion using Coix lacryma-jobi seed extract as oil phase for enhanced antitumor efficacy: preparation and in vivo evaluation. *Int J Nanomedicine*. 2014;9:109–119.
41. Liu M, Shen S, Wen D, et al. Hierarchical Nanoassemblies-Assisted Combinational Delivery of Cytotoxic Protein and Antibiotic for Cancer Treatment. *Nano Lett*. 2018;18(4):2294–2303.
42. Firempong CK, Zhang HY, Wang Y, et al. Segetoside I, a plant-derived bisdesmosidic saponin, induces apoptosis in human hepatoma cells in vitro and inhibits tumor growth in vivo. *Pharmacol Res*. 2016;110:101–110.
43. Obchoei S, Saeeng R, Wongkham C, Wongkham S. Novel Synthetic Mono-triazole Glycosides Induce G_0/G_1 Cell-cycle Arrest and Apoptosis in Cholangiocarcinoma Cells. *Anticancer Res*. 2016;36(11):5965–5974.
44. Li P, Zhou X, Qu D, et al. Preliminary study on fabrication, characterization and synergistic anti-lung cancer effects of self-assembled micelles of covalently conjugated celastrol-polyethylene glycol-ginsenoside Rh2. *Drug Deliv*. 2017;24(1):834–845.
45. Wilhelm S, Tavares AJ, Dai Q, et al. Analysis of nanoparticle delivery to tumours. *Nat Rev Mater*. 2016;1(5):16014.
46. Wang J, Mao W, Lock LL, et al. The Role of Micelle Size in Tumor Accumulation, Penetration, and Treatment. *ACS Nano*. 2015;9(7):7195–7206.
47. Li P, Nijhawan D, Budihardjo I, et al. Cytochrome c and dATP-dependent formation of Apaf-1/caspase-9 complex initiates an apoptotic protease cascade. *Cell*. 1997;91(4):479–489.
48. Amirghofran Z, Daneshbod Y, Gholijani N, Esmaeilbeig M. The influence of Bcl-2 and myeloid antigen expression on response to therapy in childhood acute lymphoblastic leukemia. *Arch Iran Med*. 2011;14(3):170–174.
49. Chipuk JE, Kuwana T, Bouchier-Hayes L, et al. Direct activation of Bax by p53 mediates mitochondrial membrane permeabilization and apoptosis. *Science*. 2004;303(5660):1010–1014.
50. Shih HC, Shiozawa T, Kato K, et al. Immunohistochemical expression of cyclins, cyclin-dependent kinases, tumor-suppressor gene products, Ki-67, and sex steroid receptors in endometrial carcinoma: positive staining for cyclin A as a poor prognostic indicator. *Hum Pathol*. 2003;34(5):471–478.
51. Stark GR, Taylor WR. Control of the G2/M transition. *Mol Biotechnol*. 2006;32(3):227–248.
52. Xiao B, Spencer J, Clements A, et al. Crystal structure of the retinoblastoma tumor suppressor protein bound to E2F and the molecular basis of its regulation. *Proc Natl Acad Sci U S A*. 2003;100(5):2363–2368.
53. Müller-Tidow C, Metzger R, Kügler K, et al. Cyclin E is the only cyclin-dependent kinase 2-associated cyclin that predicts metastasis and survival in early stage non-small cell lung cancer. *Cancer Res*. 2001;61(2):647–653.
54. van Dilla MA, Trujillo TT, Mullaney PF, Coulter JR. Cell microfluorometry: a method for rapid fluorescence measurement. *Science*. 1969;163(3872):1213–1214.

Supplementary materials

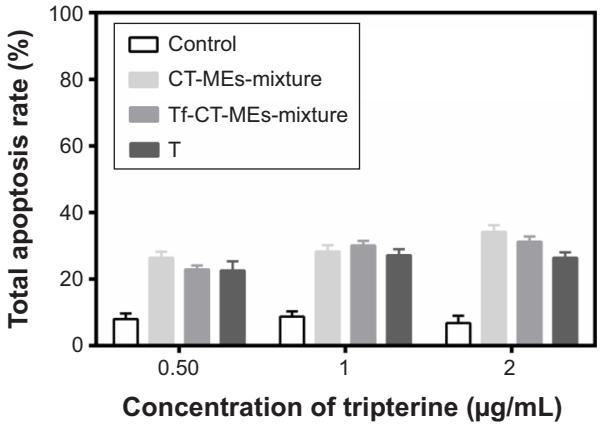

Figure S1 Cytotoxicity of different treatments of excipients against HeLa cells for 4 hours (n=3).
Abbreviations: CT-MEs, tripterine-loaded coix seed oil microemulsion; Tf-CT-MEs, transferrin-modified tripterine-loaded coix seed oil microemulsion; T, tripterine.

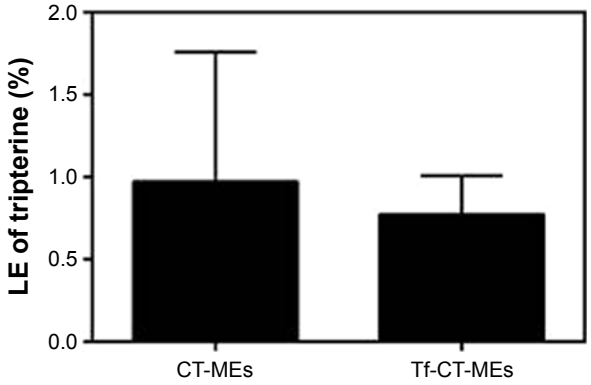

Figure S2 Drug LE of tripterine in CT-MEs and Tf-CT-MEs.
Abbreviations: LE, loading efficiency; Tf-CT-MEs, transferrin-modified tripterine-loaded coix seed oil microemulsion.